Effect of Nonlinear Surface Inflows into Activity Belts on Solar Cycle Modulation

Mohammed H. Talafha[1,2] [ID] · **Kristóf Petrovay[3]** [ID] · **Andrea Opitz[1]** [ID]

Abstract Converging flows are visible around bipolar magnetic regions (BMRs) on the solar surface, according to observations. Average flows are created by these inflows combined, and the strength of these flows depends on the amount of flux present during the solar cycle. In models of the solar cycle, this average flow can be depicted as perturbations to the meridional flow. In this article, we study the effects of introducing surface inflow to the surface flux transport models (SFT) as a possible nonlinear mechanism in the presence of latitude quenching for an inflow profile whose amplitude varies within a cycle depending on the magnetic activity. Using a grid based on one-dimensional SFT models, we methodically investigated the extent of nonlinearity caused by inflows, latitude quenching (LQ), and their combinations. The results show that including surface inflows in the model in the presence of both LQ and tilt quenching (TQ) produced a polar field within a $\pm 1\sigma$ of an average cycle polar field (σ is the standard deviation) and a correlation coefficient of 0.85. We confirm that including inflows produces a lower net contribution to the dipole moment ($10-25\%$). Furthermore, the relative importance of LQ vs. inflows is inversely correlated with the dynamo effectivity range (λ_R). With no decay term, introducing inflows into the model resulted in a less significant net contribution to the dipole moment. Including inflows in the SFT model shows a possible nonlinear relationship between the

✉ M. H. Talafha
mtalafha901@gmail.com

K. Petrovay
k.petrovay@astro.elte.hu

A. Opitz
opitz.andrea@wigner.hu

[1]   HUN-REN Wigner Research Centre for Physics, Department of Space Physics and Space Technology, Budapest, Hungary

[2]   Research Institute of Science and Engineering, University of Sharjah, Sharjah, UAE

[3]   ELTE Eötvös Loránd University, Institute of Geography and Earth Sciences, Department of Astronomy, Budapest, Hungary

surface inflows and the solar dipole moment, <u>suggesting a potential nonlinear mechanism contributing to the saturation of the global dynamo.</u> For lower λ_R ($\lesssim 10°$), TQ always dominates LQ, and for higher λ_R LQ dominate. However, including inflows will make the domination a little bit earlier in case of having a decay term in the model.

Keywords: Magnetic fields, Models; Magnetic fields, Photosphere; Magnetohydrodynamics; Solar Cycle, Models.

1. Introduction

Solar dynamo models describe the evolution of solar cycles over time, with poloidal and toroidal fields as the main components in a Babcock-Leighton (BL) dynamo model. Poloidal fields wind up by differential rotation to form the toroidal fields of the next cycle, and the toroidal field serves as seeds for the poloidal field (Bhowmik et al. 2023). Surface flux transport models (SFT) have been used to describe these large-scale photospheric magnetic fields' evolution by assuming that the surface field is nearly radial. Its evolution can be represented by the radial component of the magnetohydrodynamics (MHD) induction equation, where advection is attributed to differential rotation and poleward meridional flow and diffusion to the mixing action of supergranular flows (Yeates et al. 2023). The reversal of the polar field and solar dipole moment in the middle of the activity cycles originates from the systematic latitude-dependent tilt of the active regions (ARs) relative to the azimuthal direction (Joy's law) and can be reproduced by the SFT. In addition, Schrijver, De Rosa, and Title (2002) introduced a decay term to solve the problem of dipole moment drift. SFT models were used in literature for simulating and modelling the solar magnetic field (Cameron et al. 2012; Cameron and Schüssler 2016; Jiang et al. 2011; Whitbread et al. 2017); in addition to solar cycle prediction (Jiang et al. 2018; Iijima et al. 2017; Jiang 2020; Petrovay 2020), a recent review of the model given by Yeates et al. (2023).

The generation of the toroidal magnetic field is linearly linked to the strength of the poloidal field during the minimum of the previous cycle (Jiang et al. 2018). However, it is anticipated that the transformation of the toroidal field into the poloidal field through the BL mechanism is a nonlinear process, which plays a significant role in the amplified growth of amplitude and variability of the solar cycle.

The tilt angle of the sunspot group plays a vital role in the formation of the poloidal field generated by the toroidal field through the BL mechanism. As a sunspot group develops across the solar surface, its tilt angle changes over time. Analysing its characteristics at various stages of evolution provides insight into the physical origins of tilt angles. According to the thin flux-tube model of BMR formation, the tilt is thought to result from the Coriolis force acting on the rising flux tube of the strong toroidal magnetic field originating at the base of the convection zone (Jha et al. 2020). The scatter in the tilt angle arises from two factors, one of which is the generation mechanism of the tilt angle,

potentially influenced by turbulent convection. The other factor contributing to tilt angle scatter is measurement errors, such as those arising from measurements conducted in unipolar regions. Studying tilt angles aids in uncovering the mechanisms behind the randomness of the solar cycle and provides insights into flux tube emergence (Jiao, Jiang, and Wang 2021).

The thin-flux-tube approximation theory posits that as the field strength rises, there is a decrease in tilts, which implies a nonlinear feedback mechanism that affects the efficiency of the BL mechanism (D'silva and Choudhuri 1993). Dasi-Espuig et al. (2010) conducted a study that revealed a noteworthy association between the average tilt of bipolar active regions and the amplitude of the solar cycle. This correlation, commonly referred to as tilt-quenching (TQ), has been widely incorporated into solar dynamo models. Importantly, they found that the product of the mean tilt and cycle amplitude was a reliable predictor of the amplitude of the subsequent solar cycle. This finding holds significance in the context of understanding and forecasting solar activity dynamics. This correlation was confirmed by Jiao, Jiang, and Wang (2021) through a comprehensive examination of the existing methodologies employed to estimate tilt angles using data from the Kodaikanal and Mount Wilson observatories. In addition, the tilt angles from the Debrecen photoheliographic dataset were incorporated into the analysis. Meticulous analysis revealed a significant inverse correlation between the tilt angles and the strength of the solar cycle. Using line-of-sight magnetograms obtained from the Michelson Doppler Imager (MDI) aboard the Solar and Heliospheric Observatory (SOHO) covering the period 1996-2011, as well as the Helioseismic and Magnetic Imager (HMI) aboard the Solar Dynamic Observatory (SDO) from 2010 to 2018. Jha et al. (2020) investigated the tilt characteristics of Bipolar Magnetic Regions (BMRs) within a solar cycle and demonstrated that the tilt of BMRs exhibits a nonmonotonic relationship with the field strength of the region. Specifically, the tilt angle increased in the small magnetic field regime, whereas it decreased in the large magnetic field regime.

The efficiency of poloidal field generation by BMRs diminishes when they emerge at higher latitudes, mainly because of the limited cross-equatorial cancellation (Jiang et al. 2014). Cross-equatorial transport is indispensable for the buildup of the new poloidal field in the Babcock-Leighton scenario. Without cross-equatorial transport, there would be simply no polar reversal, and no new cycle would follow (Petrovay 2020). For clarification, the cross-equatorial transport discussed in this article is not related to the positions or proper motions of ARs: it is a diffusive transport of the large-scale mean-field, for which direct evidence would be hard to find. The overall agreement of the evolution of the large-scale solar magnetic field with SFT model predictions is, however, strong indirect evidence for cross-equatorial transport (Yeates et al. 2023). However, when a BMR emerges in proximity to the equator, the process of cancelling out the leading polarities with a flux of opposite polarity from the other hemisphere is facilitated. Jiang (2020) directed attention towards "latitude quenching" (LQ), as this nonlinear modulation mechanism is coined by Petrovay (2020). The LQ was derived from an empirical observation made through extensive analysis of a long sunspot record, revealing a correlation between the average latitude of the active region appearance during a specific phase of the solar cycle and the

amplitude of the cycle (Jiang et al. 2011). The presence of active regions at higher latitudes hampers the diffusion of the leading flux across the equator, consequently reducing the contribution of the trailing flux to polar fields. Consequently, the observed negative correlation between the average latitude of active region emergence and the cycle amplitude signifies the presence of a negative feedback effect. Karak (2020) argued that LQ can effectively govern the growth of the magnetic field, particularly when the dynamo operates within a moderately supercritical regime, by incorporating this concept into a 3D Babcock–Leighton dynamo model using a straightforward latitude-dependent threshold for BMR eruption.

Talafha et al. (2022) conducted a comprehensive investigation to assess the influence of the two potential nonlinearities, TQ and LQ, on the source term in an SFT model systematic simulation. Both TQ and LQ serve as plausible saturation mechanisms that explain the absence of the runaway exponential growth in the solar dynamo. The study revealed that the relative impact of TQ versus LQ on the axial dipole at the end of the solar cycle is primarily determined by the dynamo effectivity range λ_R, defined as a universal function of Δ_u/η, where Δ_u is the divergence of the meridional flow at the equator and η represents the diffusivity; Eqs. (26) and (27) in Petrovay, Nagy, and Yeates (2020). Specifically, when λ_R is small, LQ exhibits a greater reduction in the end-of-cycle axial dipole than TQ. Conversely, for large values of λ_R, TQ is more influential than LQ in diminishing the end-of-cycle dipole.

Observations on the solar surface reveal the presence of converging flows surrounding BMRs (Gizon, Duvall, and Larsen 2001; González Hernández et al. 2008). These inflows collectively generate average flows around the activity belt, and their intensity is contingent on the level of flux within the solar cycle, as demonstrated by Jiang et al. (2010) and Cameron and Schüssler (2012). The average poleward meridional flow experiences a modest change of approximately 25% between the maximum and minimum phases of the solar cycle, or from one cycle to another (Komm, Howard, and Harvey 1993; Hathaway and Rightmire 2010). This variation is attributed, at least in part, to surface inflows directed towards large active regions (Gizon 2004; Cameron and Schüssler 2010; Jiang et al. 2010). These inflows can reach a substantial fraction of the mean axisymmetric poleward meridional flow at mid-latitudes, but their spatial extent remains confined to the belts where the active regions are located. The magnetic influence on surface flows can induce variations in the transportation of magnetic flux towards the pole, consequently affecting the dynamo efficiency of decaying bipolar active regions. This alteration leads to a reduction in the cross-equatorial cancellations of BMRs and suppresses the effectiveness of the Babcock–Leighton process. In the case of a strong solar cycle, this effect becomes more pronounced and imparts a stabilising influence on the dynamo, as demonstrated by Martin-Belda and Cameron (2017) and Nagy, Lemerle, and Charbonneau (2020).

This study aims to investigate how surface inflows towards active-region belts affect solar cycle modulation as a quenching mechanism for the solar dynamo. In particular, we employ the model formulation introduced by Jiang et al. (2010) and its subsequent modifications in Nagy, Lemerle, and Charbonneau (2020) by imposing axisymmetric bands of converging latitudinal flow as perturbations

of meridional flow. The novelty in the current paper is the addition of the meridional inflow as opposed to either TQ or LQ .

The remainder of this paper is organized as follows. In Section 2, we provide a detailed description of the SFT model used in this study and describe the surface inflow profile that we use. The results of our solar cycle simulations are then presented in Section 3, regarding the modified surface inflows profile (Nagy, Lemerle, and Charbonneau 2020). The discussion is given in Section 4, and the paper is concluded in Section 5.

2. Modulation of Surface Inflows in a Surface Flux Transport Model

To investigate how surface inflows affect one-dimensional (1D) SFT models with the LQ mechanism, we used the results of Petrovay and Talafha (2019) (hereafter Paper 1) as the optimised combinations of model parameters and Talafha et al. (2022) (hereafter Paper 2) as the parameter values for LQ.

As we modelled the "average" solar cycles in papers 1 and 2, the source function is a smooth distribution that can be regarded as an ensemble average. This allowed us to simulate the probability distribution of the emergence of leading and trailing polarity on the solar surface. Because this source is axially symmetric, our entire SFT model can be simplified to one dimension, as shown in Equation 1.

$$
\begin{aligned}
\frac{\partial B}{\partial t} \;=\; & \frac{1}{R\cos\lambda}\frac{\partial}{\partial\lambda}(B\,u\,\cos\lambda) \\
& + \frac{\eta}{R^2\cos\lambda}\frac{\partial}{\partial\lambda}\left(\cos\lambda\frac{\partial B}{\partial\lambda}\right) - \frac{B}{\tau} + s(\lambda,t)
\end{aligned}
\tag{1}
$$

Where u is the meridional flow speed, τ is the timescale of decay due to radial diffusion, R is the solar radius, and η is the supergranular diffusivity. The meridional flow profile used in this work is within the observational constraints. In principle, dynamical models of meridional circulation might also be used; however, these also involve numerous ad hoc assumptions. For example, the recent numerical simulations by Finley et al. (2024) apply an arbitrary rescaling of the Nusselt number, given the convective conundrum, and they neglect the magnetic feedback. For our study, a dynamic model would be an unnecessary complication that would not make the flow pattern more unique.

The source term s represents flux emergence by a general form of ring pairs with opposite magnetic polarity, as described by Talafha et al. (2022); in this work, we only considered the LQ effects (i.e., the b_{joy} parameter is equal to zero).

As explained in detail in the recent review by Yeates et al. (2023), the SFT equation is the radial component of the magnetic induction equation at the surface where the radial diffusion term is either neglected or represented in a simplified way (decay term with parameter in τ our case). A more realistic form for this term was given by Baumann et al. (2004). According to one widely

held view, the strong downwards-directed pumping in the shallow layers may make this contribution insignificant (see Ossendrijver et al. (2002); Käpylä et al. (2006), and references therein). Apart from this simplification, the SFT equation is exact. Radial flows have no direct relevance to the redistribution of the radial magnetic field on the solar surface.

Surface inflows were added as perturbations to the meridional flow $\Delta v(\lambda, t)$ as the axisymmetric parametric form introduced by Jiang et al. (2010), but their amplitude varies over time within a cycle depending on the magnetic activity (Nagy, Lemerle, and Charbonneau 2020). In a full non-axisymmetric model, the inflows should be centred on individual active regions. As, however, our study focuses on solar cycle modulation, which is determined by the axial dipole moment built up by the end of the cycle, it is sufficient in this work to consider the azimuthally averaged SFT equation. The assumed latitudinal inflows result from the azimuthal averaging of the actual radial inflows towards ARs; hence, their amplitude is expected to scale with the number of ARs present and their time scale is comparable to the cycle length. Just as the time scale of the source term s is the cycle time rather than the lifetime of individual ARs. For the specific form (Equation 3) used for the scaling and the value of the amplitude parameter v_{00}, we follow Nagy, Lemerle, and Charbonneau (2020)

$$\Delta v(\lambda, t) = \begin{cases} -v_0 \sin(\frac{\lambda - \lambda_0(t)}{\delta\lambda}) & \text{if } -\pi < \frac{\lambda - \lambda_0(t)}{\delta\lambda} < \pi \\ 0 & \text{otherwise} \end{cases} \qquad (2)$$

Here, the velocity amplitude of the bands $v_0(t)$ is calculated as follows:

$$v_0(t) = v_{00} \cdot \arctan\left(\frac{S_n}{F_{00}}\right) \qquad (3)$$

S_n is the scaled cycle amplitude and $F_{00} = 4.99 \times 10^{-21}$, is an arbitrary normalisation parameter, the initial amplitude of the inflows, $v_{00} = -500$ and -750 cm s^{-1}. The dependence of the arctangent in Equation 3 prohibits unreasonably high inflow speeds for rogue BMR emergencies (Nagy et al. 2017). In these bands, $\delta\lambda$ is the width of the bands, and λ_0 is its central latitude. We obtain another band in the opposite hemisphere by substituting $\lambda_0 \rightarrow -\lambda_0$. For sufficiently small central latitudes, the two bands can overlap, and the corresponding velocities are added. The temporal dependency of $\lambda_0(t; i)$, Equation 4, represents the equatorward travel of the bands during the solar cycle. The width of the bands $\delta\lambda$ follow the standard deviation in Equation 5

$$\lambda_0(t; i)[°] = [26.4 - 34.2(t/P) + 16.1(t/P)^2](\lambda_i/14.6) \qquad (4)$$

$$\delta\lambda = [0.14 + 1.05(t/P) - 0.78(t/P)^2]\lambda_0 \qquad (5)$$

where $P = 11$ year is the cycle period. From the point of view of our axisymmetric model, what matters is not the tilt angle by itself but the latitude difference between the leading and trailing polarities. This is not affected by differential

Table 1. Set of parameters considered for inflows with the Surface inflows whose amplitudes vary within a cycle depending on the magnetic activity and its deviations $|\Delta D_n|$ of the nonlinear models from the linear case measured at a certain SSN value. The surface inflow initial amplitude $v_{00} = -500$ cm s^{-1}.

Case	u_0 [m s^{-1}]	η [km^{2}s^{-1}]	τ [yr]	dev LQ+inflows	dev$_{LQ}$	dev inflows
a	11	250	8	2.410	1.614	1.149
b	11	350	8	2.874	1.429	1.722
c	11	450	8	3.087	1.083	2.290
d	11	550	8	3.032	0.729	2.337
e	11	650	8	2.956	0.604	2.460
f	11	250	∞	2.263	1.422	1.051
g	11	350	∞	2.471	1.334	1.389
h	11	450	∞	2.372	1.077	1.469
i	11	550	∞	2.1621	0.763	1.445
j	11	650	∞	2.040	0.637	1.331

rotation. Following usual practice, in our SFT model, the AR source is introduced instantaneously, and its further evolution is described by the SFT model.

The amplitude of the inflows was scaled to depend on the cycle amplitude A_n, as $(A_0\text{-}A_n)\times 10$. The constant A_0 was assigned a value of $0.001\,exp(7[yr]/\tau)$ to ensure that the resulting dipolar moments aligned reasonably well with the observed values (measured in Gauss) for an average cycle. Note that with this scale and τ-dependence, defining $S_n = \chi\,A_n s_1$ yields values of S_n comparable to the observed sunspot numbers (SSN), where χ is a dimensionless parameter equal to 400 for $\tau = 8$ years and 1000 for $\tau = \infty$, which ensures that the average S_n is identical to the average observed values.

For the SFT model parameters, our model grid was a subset of the grid described in Paper 1. For τ, we only consider two values; a decay time scale of 8 years, comparable to the cycle length and supported by several studies (see Paper 1 and references therein), and a decay time scale of ∞, so no decay term. The meridional flow amplitude was set to $u_0 = 11$ m s^{-1}, and the initial amplitudes of the inflow were $v_{00} = -500$ and -750 cm s^{-1}, across various parameter combinations as detailed in Tables 1 and 2, respectively. The parameters were constrained in the range allowed by observations, and within this range, a limited mapping of the parameter space was performed. These combinations correspond to two distinct initial inflow amplitudes, as suggested by Nagy, Lemerle, and Charbonneau (2020). This approach allows us to demonstrate the impact of surface inflows with higher initial amplitudes.

Table 2. Same as Table 1, with the initial surface inflow amplitude $v_{00} = -750$ cm s^{-1}.

Case	u_0 [m s^{-1}]	η [km^{2}s^{-1}]	τ [yr]	dev LQ+inflows	dev$_{LQ}$	dev inflows
k	11	250	8	2.024	1.614	0.996
l	11	350	8	2.785	1.429	1.835
m	11	450	8	3.167	1.083	2.413
n	11	550	8	3.14	0.729	2.503
o	11	650	8	3.118	0.604	2.731
p	11	250	∞	2.173	1.422	1.062
q	11	350	∞	2.557	1.334	1.536
r	11	450	∞	2.571	1.077	1.689
s	11	550	∞	2.409	0.763	1.682
t	11	650	∞	2.381	0.637	1.787

3. Results

As the migrating flow perturbation represents a strong non-uniform latitudinal variation in the divergence of the flow, the problem at hand does not lend itself to the simplified analytic treatment applied in Talafha et al. (2022). Hence, the analytic fits to the results of our numerical exploration of the problem are simply based on a generalization of the results obtained by Talafha et al. (2022).

To investigate the effect of introducing surface inflows into the model, we first look into the impact of the surface inflows on the polar field for different setups (inflows, LQTQ, LQTQ+inflows) and compare it with an average cycle polar field. After that, we studied the model deviations in the net contribution of a cycle to the dipole moment $|\Delta D_n|$ for the three nonlinear scenarios (inflows, LQ and inflows+LQ) from the linear case (no LQ+ no inflows). Finally, we check the domination of LQ over TQ in the presence of surface inflows.

3.1. Polar Field for Ten Solar Cycles

The polar field reverses by the end of every solar cycle, a process suggested by Babcock and Babcock (1955) due to the magnetic flux transport on the solar surface. Correlation between the polar field at cycle minimum and the next cycle amplitude maximum confirmed by several studies (Wang and Sheeley 2009; Hathaway and Upton 2016), this makes the polar field a precursor of cycle strength (Petrovay 2020).

Using the 1D SFT model described earlier, we look into the polar field for 10 solar cycles, considering the two nonlinear mechanisms, Latitude and tilt quenching (LQ and TQ), in addition to the surface inflows as a possible nonlinearity. First, we simulate an average solar cycle as in paper 1, adding both LQ and TQ to the model as in paper 2 and, finally, including the surface inflows.
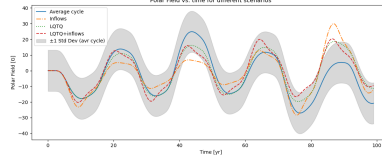
Figure 1. Polar field [G] *vs.* Time [yr] for 10 average solar cycles (solid blue), including inflows (dash-dotted orange), latitude and tilt quenching (dotted green) and all of the three mechanisms to the average cycle (dashed red). A $\pm 1\sigma$ of the average cycle is shown as the shaded area.
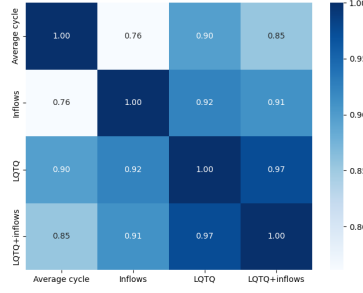

Figure 2. Correlation matrix illustrating the relationships between different cases. The matrix highlights the degree of correlation between parameters of the average cycle, inflows, latitude and tilt quenching (LQTQ), and combined (LQTQ+Inflows) scenarios. Higher values indicate stronger correlations, while lower values indicate weaker correlations.

The model parameters considered in this article are based on the optimisation results in paper 1. For meridional flow amplitude, $u_0 = 11$ m s^{-1}, diffusivity η was set to 250 km^{2}s^{-1} and the decay time scale for $\tau = 8$ yr. For latitude quenching (LQ), the b_{lat} parameter was set to 2.4, and for tilt quenching (TQ), the b_{joy} parameter was set to 0.15.

The polar field values for different scenarios were calculated, firstly, polar field values for an average solar cycle, no quenching mechanisms and no inflows (average cycle), secondly, the average solar cycle with inflows (inflows), a third scenario to include both LQ and TQ with the average cycle polar field (LQTQ), and lastly to consider all the mechanisms together (LQTQ+inflows). Figure 1 shows the polar field for 10 solar cycles for these different scenarios with time. A 1 Standard deviation (σ) is shown for the average cycle, the other three scenarios were nearly laying in between $\pm\sigma$, except for the last cycle which shows a slight deviation.

The correlation of the different scenarios with the average solar cycle is shown in Figure 2, it's important to say that the LQTQ scenario correlates with the average cycle by 0.9 factor, however, including the inflows to the model in addition to LQ and TQ reduces the correlation factor to 0.85.

The polar field for the average solar cycle was fitted to a harmonic function of the form:

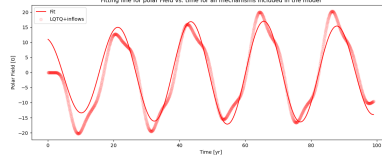$$f(t) = (a_0 + a_1 t + a_2 t^2)\sin(bt + c) \tag{6}$$

Figure 3. Fitting line for polar field vs. time for all mechanisms (LQTQ + inflows) case included in the model for 10 solar cycles, fitting parameters listed in Table 3

where a_0, a_1, a_2, b and c are fitting parameters. The choice of this form was selected based on the varying amplitudes of the polar field through the 10 cycles in addition to its periodic nature. As an example, Figure 3 shows the case where all of the three mechanisms considered (LQTQ+inflows) in the model, the polar field values were fitted to the form in Equation 6, the complete list of the fitting parameters best values for each scenario given in Table 3.

Table 3. Fitting parameters of polar field vs. time for different cases

Case	a_0	a_1	a_2	b	c
Average cycle	-8.986	-0.407	0.004	0.284	-1.54
LQ	-6.404	-0.378	0.003	0.284	-1.543
TQ	-10.583	-0.168	0.002	0.281	-1.417
Inflows	-14.592	0.282	-0.004	0.28	-1.145
LQTQ	-9.296	-0.274	0.002	0.283	-1.453
LQTQ+inflows	-11.587	-0.197	0.002	0.282	-1.27

To compare each scenario with the average cycle, we calculate the percentage error between the fitting parameters of each scenario and the average cycle. Table 4 shows the percentage error for each parameter in Equation 6. The "Inflows" scenario consistently shows the largest percentage errors across most parameters, particularly for a_1 (169.29%), a_2 (200.00%), and a_0 (62.38%), this proves that the inflows significantly impact the parameters compared to the other scenarios. The parameter b remains relatively stable across all scenarios, with the percentage errors being minimal (ranging between $0.00-1.41\%$), which suggests that b is less sensitive to the variations in the different cases studied. All scenarios show notable percentage errors in a_0, but "Inflows" shows the largest positive percentage error; this parameter seems to be highly influenced by the inclusion of inflows. The combined cases (LQTQ and LQTQ+Inflows) generally show moderate percentage errors from the average cycle values, this suggests that the combined effects of Latitude and tilt quenching, as well as inflows, lead to a more balanced impact on the parameters. There is significant variation in parameter c, especially for "Inflows" (25.65%), indicating that the inflow case has a substantial impact on this parameter, differentiating it from other scenarios.

Table 4. Percentage error of fitting parameters for different cases compared to the average cycle.

Case	$\Delta a_0(\%)$	$\Delta a_1(\%)$	$\Delta a_2(\%)$	$\Delta b(\%)$	$\Delta c(\%)$
LQ	28.74	7.12	25.00	0.00	0.19
TQ	17.77	58.72	50.00	1.06	7.99
Inflows	62.38	169.29	200.00	1.41	25.65
LQTQ	3.45	32.68	50.00	0.35	5.65
LQTQ+Inflows	28.94	51.60	50.00	0.70	17.53

3.2. Surface Inflows as a Nonlinearity in the SFT Model

The surface inflows can be represented by adding perturbations to the meridional flow profile. Nagy, Lemerle, and Charbonneau (2020) utilised the model framework proposed by Jiang et al. (2010), introducing modifications to the width and speed of the inflow to ensure their proportionality to the emerging magnetic flux. However, in this article, we consider this profile to be dependent on the cycle amplitude, as described in the previous section. This modification transformed the inflows into an authentic nonlinear magnetic response mechanism rather than imposing predetermined latitudinal profiles and inflow speeds.

We aim to obtain a statistically meaningful sample of solar cycles by solving the azimuthally averaged SFT equation, Equation 1, for 1000 cycles, by varying the parameters η, τ and v_0 as listed in Tables 1 and 2. As an illustration, Figure 4 shows the net contribution of a solar cycle to the solar dipole moment plotted against the cycle amplitude. This comparison was performed in the presence and absence of surface inflows. Defining $r = e^{-11/\tau}$ (with τ in years), the net contribution of the cycle n to the change in the dipolar moment is given by $\Delta D_n = D_{n+1} - rD_n$, where D_n represent the dipole moment for the cycle n at cycle minimum as defined in paper 2.

TQ was not considered here because it might overestimate the effects of nonlinearities if both tilt quenching and inflows are incorporated into the surface flux transport process. The decision to exclude TQ and concentrate on LQ and inflows was motivated by our hypothesis that inflows may be responsible for tilt quenching. Inflows could play a significant role in the tilt-quenching process; larger tilt angles indicate that stronger inflows are required to obtain regular polar field reversals in SFT models, which brings new constraints on the amplitudes of inflow (Jiao, Jiang, and Wang 2021). Martin-Belda and Cameron (2016) investigated the role of the converging flows towards a BMR in its evolution and their impact on the axial dipolar field, they found that the latitudinal separation of the polarities of the bipolar region is limited by the inflows, resulting in a reduction of the axial dipole moment of the BMR, and hence, lowers the contribution of the emerged BMR to the axial dipole moment. Therefore, to avoid the potential overestimation of nonlinear effects by incorporating both TQ and inflows into the SFT process, we examined the effects of LQ and inflows while excluding TQ.
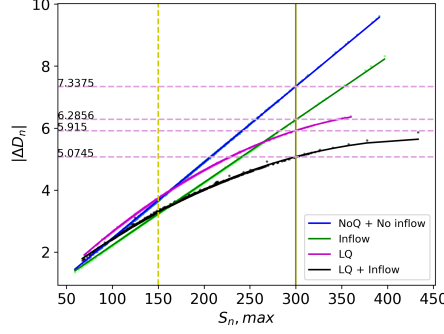
Figure 4. Net contribution of a cycle to the solar dipolar moment vs. cycle amplitude for the different cases to the linear case with no quenching. The parameter values were $u_0 = 11$ m/s, $\eta = 250 \, \text{km}^2\text{s}^{-1}$ and $\tau = \infty$ years. inflows are implemented with an initial amplitude $v_00 = -500$ cm s^{-1}. The dashed and solid vertical lines show the average and twice average cycle amplitude values respectively, and the horizontal dashed lines show where the twice average vertical line intersects with each case.

Deviations from the linear case (no inflows + no LQ) were calculated at an arbitrarily selected value of S_n (approximately twice the mean), as indicated by the solid vertical line in this figure. Table 1 shows the deviations of the inflows, LQ, and inflows+LQ from the linear case (no inflows + no LQ), for example, in Figure 4, $dev_{inflows} = 7.335\text{-}6.285 = 1.051$.

The average S_{max} was set to 150 based on the literature. Therefore, for each parameter combination, S_n, max was scaled using χ to obtain values comparable to the observed sunspot number SSN. For various cases (a-t), it is evident that these deviations are significantly influenced by the selection of u_0, η, and τ. The linear case (no inflows + no LQ) was fitted with a linear function, whereas the other three cases were fitted with quadratic polynomials following the results in paper 2.

Including inflows in the model resulted in a decreased net contribution to the solar dipole moment in all cases, as shown in Figure 4. For both linear and LQ cases, having inflows in the model diminished the overall cycle contribution to the solar dipole moment, as indicated by the dev_{inflows} and $dev_{\text{LQ+inflows}}$ in Tables 1 and 2.

Figure 5 shows the relative importance of LQ vs. inflows for different parameter combinations plotted against u_0/η and fitted to a quadratic polynomial of the form:

$$dev_{\text{LQ}}/dev_{\text{inflows}} = c_1(u_0/\eta)^2 + c_2(u_0/\eta) + c_3 \tag{7}$$

where c_1, c_2, and c_3 are the fitting parameters that depend on τ. Note that the relative importance of the LQ vs. inflows for $\tau = 8$ is always higher than that for $\tau = \infty$; that is, with no decay term, inflows will be less significant. Using two initial inflow amplitudes v_{00}, introducing the surface inflows with $v_{00} = -750$ cm s^{-1} gave lower relative importance of LQ vs. inflows than using $v_{00} = -500$ cm s^{-1} for both $\tau = 8$ and ∞. To assess whether the fitting parameters c_1, c_2 and c_3 differed significantly between the two inflows amplitudes $v_{00} = -500$ cm s^{-1} and $v_{00} = -750$ cm s^{-1}, we conducted paired t-tests for each parameter.
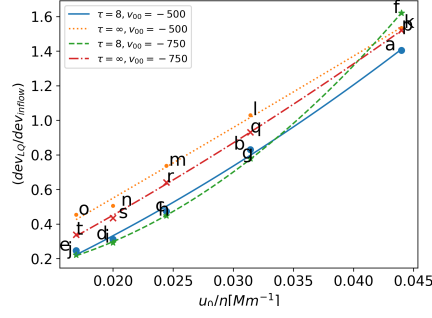
Figure 5. The relative importance of LQ vs. inflows plotted against the u_0/η ratio. Separate third-degree polynomial fits for the case $\tau = 8$ (solid blue and dashed green) and $\tau = \infty$ (dotted orange and dash-dotted red) are shown for the different parameter combinations listed in Tables 1 and 2.

The parameters were analyzed under the two values of $\tau = 8$ years and ∞. Table 5 show the t-statistics and p-values, these results indicate that there are no significant differences in the fitting parameters $c1$, $c2$, and $c3$ between the two initial inflows amplitudes for both $\tau = 8$ and $\tau = \infty$. This can be interpreted as increasing the initial inflow amplitudes produced slightly significant inflows.

Table 5. Paired t-test results for fitting parameters $c1$, $c2$, and $c3$ comparing $(v_{00} = $ -500 cm s$^{-1})$ and $(v_{00} = $ -750 cm s$^{-1})$ for both $\tau = 8$ [yr] and ∞.

Parameter	t-statistic	p-value
c_1	-1.60	0.35
c_2	1.52	0.37
c_3	-0.92	0.53

The dynamo effectivity range λ_R enabled visualization of the inherent connection between the nonlinearity ratios related to the inflows and λ_R. where λ_R defined by the empirical fit found by Petrovay, Nagy, and Yeates (2020):

$$\lambda_{R,fit} = g^{1/2}(x = \eta/R^2\Delta_u)\lambda_{R,limit} \tag{8}$$

with

$$
\begin{aligned}
g(x) &= (m_1 x + c_1)\{1 - tanh[(x - c_0)/w]\} \\
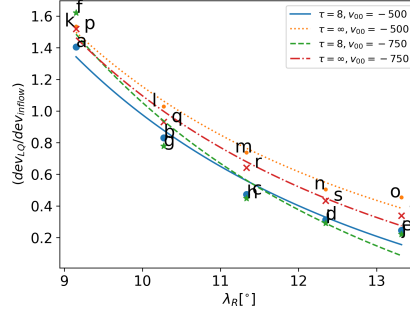&+ (m_2 x + c_2)\{tanh[(x - c_0)/w]\}
\end{aligned}
\tag{9}
$$

Figure 6. The relative importance of LQ vs. inflows plotted against the dynamo effectivity range, λ_R, for the parameter combinations listed in Tables 1 and 2. Distinct fit to Equation 11 are shown for $\tau = 8$ (solid blue and dashed green) and $\tau = \infty$ (dotted orange and dash-dotted red), respectively.

and $m_1 = 0.0004$, $m_2 = -0.0008$, $c_0 = 200$, $c_1 = 1.18$, $c_2 = 1.42$. Note that Δ_u is the divergence of the meridional flow at the equator.

$$\Delta_u = \frac{1}{R}\frac{du}{d\lambda}\big|_{\lambda=0} \tag{10}$$

Figure 6 show the relative importance of LQ vs. inflows to λ_R fitting lines for both $\tau = 8$ and $\tau = \infty$ and two initial inflows amplitudes, the fitting lines were structured according to Equation 11, for a higher amplitude of the inflow $v_{00} = -750$ cm s^{-1}, the relative importance of LQ vs. inflows is less significant for $\tau = \infty$. However, for $\tau = 8$ yr, the relative importance of LQ vs. inflows is slightly higher for low λ_R.

As a consequence of the inflows, the net flow will become convergent within a belt of half-width $\sim \delta\lambda_0$, centred on λ_0. In the absence of diffusion, the fraction f_0 of the flux in the source that falls within the convergent belt would be advected to λ_0 and cancelled. Diffusion allows a fraction f_1 of this flux to escape from the convergence belt; therefore, in the final accounting, a fraction $f = 1 - f_0(1 - f_1)$ of the flux escapes cancellation and evolves under the effect of the large-scale meridional flow and diffusion, essentially unaffected by the inflows. As f_1 depends on the inflow speed, f is modulated by the cycle amplitude. Therefore, the net effect of inflow modulation is formally reduced to the modulation of the source term in the SFT model, as in the case of tilt quenching. Therefore, we expect the effects of inflow modulation to be similar to those of the TQ. In particular, for cycle amplitudes varying in a smaller range, the resulting modulation of the source is expected to remain in the linear regime similar to the form of TQ treated in paper 1, where it was found that the relative importance of LQ and TQ will scale with the dynamo effectivity range as $C_1 + C_2/\lambda_R^2$. This prompts us to fit the curves in Figure 3 with the same fitting formulae,

$$dev_{\mathrm{LQ}}/dev_{\mathrm{inflows}} = c_1 + c_2/(\lambda_R)^2 \tag{11}$$
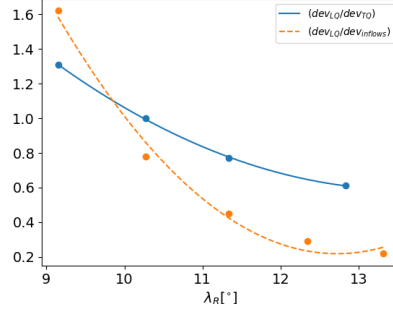
Figure 7. The relative importance of LQ vs. TQ from Talafha et al. (2022) (solid blue) and LQ vs. inflows (dashed orange) plotted against the dynamo effectivity range λ_R, for $\tau = 8$, $v_{00} = -750$ cm s^{-1}, and parameter combinations as listed in Table 2. Fit lines to a quadratic polynomial are shown as in Equation 7.

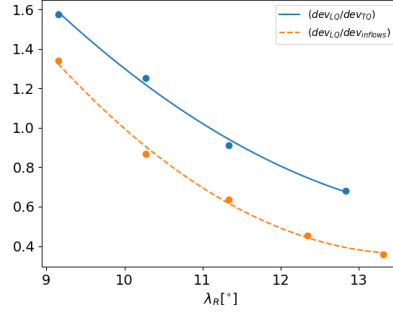**Figure 8.** Same as Figure 7 for $\tau = \infty$, $v_{00} = -750$ cm s^{-1}, and parameter combinations as listed in Table 2.

where c_1 and c_2 are fitting parameters. The fit is almost perfect. Small deviations are due to numerical errors and may be attributed to the fact that cycle amplitudes vary over a rather wide range; hence, the assumption of linear dependence of modulation of the source on cycle amplitude is rather crude.

Figure 7 and 8 show a comparison between the relative importance of TQ vs. LQ from paper 2 and the relative importance of inflows vs. LQ to λ_R for $\tau = 8$ years and ∞ respectively. The TQ and inflows exhibit similar behaviour. However, the relative importance of TQ vs. LQ is always larger than LQ vs. inflows; this supports our initial hypothesis that inflows may be responsible for tilt quenching, and hence, considering both will overestimate the effects of the nonlinearities.

3.3. Domination of LQ over TQ when considering Surface Inflows

To determine the domination of LQ over TQ we solve the azimuthally averaged SFT equation for 1000 cycles, by varying the parameters η, τ and considering no inflows in one case; $v_{00} = 0$, and with inflows in the second case; $v_{00} = -500$

Table 6. Deviations of TQ and LQ from the linear case (NoQ) for different parameter combinations for no inflows $v_{00} = 0$ and with inflows $v_{00} = -500$ cm s^{-1}.

| Case		$v_{00} = 0$			$v_{00} = -500$ [cm s^{-1}]		
η	τ	dev_{TQ}	dev_{LQ}	$[dev_{TQ} - dev_{LQ}]$	dev_{TQ}	dev_{LQ}	$[dev_{TQ} - dev_{LQ}]$
250	8	1.271	1.779	-0.508	0.911	1.051	-0.140
350	8	1.303	1.342	-0.039	1.181	1.148	0.033
450	8	1.447	1.197	0.250	1.260	1.029	0.231
550	8	1.586	0.940	0.647	1.511	1.178	0.333
650	8	1.593	0.845	0.749	1.552	0.962	0.589
250	∞	0.979	1.431	-0.452	0.941	1.378	-0.437
350	∞	1.099	1.284	-0.185	1.125	1.320	-0.196
450	∞	0.938	0.966	-0.028	1.170	1.191	-0.021
550	∞	1.121	0.719	0.403	1.203	1.099	0.104
650	∞	1.053	0.604	0.449	1.313	0.947	0.367
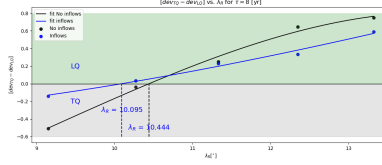
Figure 9. Difference of the deviations $(dev_{TQ} - dev_{LQ})$ plotted against λ_R for $\tau = 8$ years, fitting lines are plotted of third-degree polynomial, the vertical lines show the points of transition from TQ to LQ.

[cm s^{-1}], as listed in Table 6. The meridional flow amplitude u_0 was set as 11 [m s^{-1}] for all cases.

To investigate the effect of introducing surface inflows on the domination of LQ over TQ, we studied the model deviations of the two nonlinear scenarios (TQ and LQ) from the linear case (NoQ) for the net contribution of a cycle to the dipole moment $|\Delta D_n|$ with and without inflows. Table 6 shows these deviations and the differences of the deviations $(dev_{TQ} - dev_{LQ})$. The model was run for a range of values of $\eta \in [250 - 650]$ km^2 s^{-1}, and $\tau \in \{8, \infty\}$.

Initially, for both values of τ, dev_{TQ} is lower than dev_{LQ}, which means that the net contribution of a cycle to the solar dipole moment is higher for TQ and it dominates over LQ, by increasing the η value the net contribution of a cycle
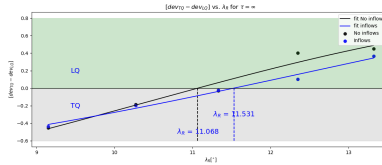

Figure 10. Same as Figure 9 for $\tau = \infty$.

to the solar dipole moment for TQ decreases gradually until the LQ dominates over TQ (at $\lambda_R = 10.44°$ for $\tau = 8$ and $\lambda_R = 11.068°$ for $\tau = \infty$). This is shown in Figures 9 and 10; the vertical lines show the points of the transitions from TQ to LQ.

Adding inflows to the model reduced the net contribution of a cycle to the solar dipole moment and this sped up the domination of LQ over TQ for $\tau = 8$ years (at $\lambda_R = 10.095°$), this can be attributed to the presence of inflows, having inflows in the SFT model reduces the flux transport toward the poles which will reduce the tilt angle and produce a lower net contribution to the dipole moment. This is not the case for $\tau = \infty$; introducing inflows to the model makes the transition from TQ to LQ slightly later in $\lambda_R = 11.531°$. This can be interpreted as $\tau = \infty$; there is no decay term, the inflows contribute to the model, and less flux cancellation occurs on the surface; this will provide more flux to the active regions and, hence, increase the tilt angle, which makes TQ dominate a little bit longer over LQ. This supports our previous result for the decay term's importance and gives evidence for our initial hypothesis that inflows might be responsible for the tilt quenching.

4. Discussion

The presence of surface inflows in solar cycle modulation, represented by perturbations to the meridional flow profile, reduces the different cycle characteristics. Cameron and Schüssler (2012) show that the magnetic flux corresponding to the axial dipole is reduced by applying strong inflows in an SFT model (Figure 2 therein). Martin-Belda and Cameron (2016) investigated the role of converging flows towards a BMR in its evolution and their impact on the axial dipolar field, they found that the latitudinal separation of the polarities of the bipolar region is limited by the inflows, resulting in a reduction of the axial dipole moment of the BMR, and hence, lowers the contribution of the emerged BMR to the axial dipole moment.

Adding inflows to the model produces a polar field within $\pm\sigma$ of the polar field of an average cycle. The correlation coefficients between the average cycle polar field and the three mechanisms were relatively high, including inflows only in the model, which gave a 0.76 correlation coefficient, and combined with LQ and TQ, which showed a 0.85 correlation coefficient. The polar field fitting parameters for considering inflows only in the model show the largest percentage of error, however, including LQ and TQ with the inflows showed a moderate percentage of error, which led to a more balanced impact on the parameters. This comes in agreement with the findings of Martin-Belda and Cameron (2017) and Nagy, Lemerle, and Charbonneau (2020) where they show that including inflows produces an alteration in the transportation of magnetic flux toward the pole and this alteration leads to a reduction in the cross-equatorial cancellations of BMRs and suppresses the effectiveness of the Babcock–Leighton process.

However, according to Nagy, Lemerle, and Charbonneau (2020), a reduction of $10-20\%$ in the strength of the global dipole as it forms towards the end of a cycle compared to a scenario without inflows, this reduction was observed

using a 2×2D Babcock–Leighton solar cycle model. Our simulation produced close results to Nagy, Lemerle, and Charbonneau (2020) by comparing the net contribution of a cycle to the solar dipolar moment with and without inflows in the absence of LQ, as in Figure 4 for example, a $12.6 - 22.8\%$ reduction in case of $v_{00} = -500$ cm s^{-1} and $10.9 - 25.4\%$ reduction for $v_{00} = -750$ cm s^{-1} using the SFT models and depending on the parameter combination, overall, when $\tau = \infty$ the reduction of the global dipole is less than the cases with $\tau = 8$ years.

Using the surface inflow profile influenced by the total emerged magnetic flux from the past cycle, Nagy, Lemerle, and Charbonneau (2020) adjusted the width and speed of the inflow to be directly related to the emerging magnetic flux, effectively transforming them into a valid nonlinear magnetic feedback mechanism. Figure 6 shows the relative importance of LQ vs. inflows plotted against the dynamo effectivity range, λ_R, for $\tau = 8$, the relative importance of LQ vs. inflows always dominated by the values for $\tau = \infty$, which was the same of the relative importance of LQ vs. TQ (as illustrated in Figure 4, paper 2). This indicates that surface inflows are strongly affected by the presence of a decay term regarding the initial inflow amplitude. As discussed earlier in Section 3, the net flow will become convergent within a belt of half-width $\delta\lambda_0$ centred on λ_0, and for strong diffusion, the escaped fraction of the flux from the convergent belt f_1 will increase, which means less flux escape cancellation f. This can be seen in the $dev_{inflows}$ values, which decrease with increasingly strong radial diffusion. On the other hand, the evolved flux under the effect of large-scale meridional flow and diffusion increases the latitude quenching mechanism, which can explain the increase in dev_{LQ} with stronger diffusion.

Figure 6 shows the relative importance of LQ vs. inflows against λ_R; fits of the form $C_1 + C_2/\lambda_R^n$ were attempted, with different integer values for n, where $n = 2$ was found to produce a reasonably good representation of the results. This agrees with the results paper 2 for the relative importance of LQ vs. TQ, which show similar behaviour, suggesting that LQ is dominant over surface inflows in the absence of TQ. This similarity is illustrated in Figs. 7 and 8. However, the relative importance of TQ vs. LQ is always greater than the relative importance of LQ vs. inflows to λ_R, which implies that a fraction of the TQ nonlinearities can be attributed to the inflow effects and also supports our hypothesis that inflows might be responsible for TQ.

The relative importance of LQ vs. inflows for the different sets of parameters (roughly between 0.2 and 1.6) was similar to the relative importance of LQ vs. TQ. However, the relative importance of LQ vs. TQ is between 0 and 2, with some negative values. Most of the SFT and dynamo models studied in the recent literature (Bhowmik and Nandy 2018; Jiang and Cao 2018; Lemerle and Charbonneau 2017; Whitbread et al. 2017), were in the range of 1 – 2. This can be explained by examining the amplitude of the surface inflow; having inflow amplitudes depending on the cycle amplitude means that we will have a lower net contribution to the dipole moment (Figure 4), which results in higher inflows deviations (dev_{inflows}), and the relative importance of LQ vs. inflows decrease.

The nonlinear relationship between the relative importance of LQ vs. inflows to the dynamo effectivity range λ_R is evident as illustrated in Figure 6 for various

combinations of parameters. The fitted lines demonstrate an inverse proportionality between λ_R and the relative importance of LQ vs. inflows, as modelled by Equation 11. This underscores the nonlinear nature of surface inflows as a truly nonlinear mechanism.

An analysis using a paired t-test on the fitting parameters for both values of v_{00} showed no significant differences. This indicates that varying the initial amplitude of the inflow has only a minor effect on the importance of the inflows.

For lower values of λ_R, TQ dominates over LQ with and without including surface inflows, by increasing λ_R gradually, a smooth transition for LQ to be dominating the TQ. This come in agreement with paper 2, where it was shown that when λ_R is small, LQ exhibits a greater reduction in the end-of-cycle axial dipole than TQ and conversely, for large values of λ_R, TQ is more influential than LQ in diminishing the end-of-cycle dipole. However, including inflows makes this transition occur faster for $\tau = 8$ yr. However, for no decay term ($\tau = \infty$), TQ dominate a little bit longer over LQ.

We reiterate that the parameter study in the present work is somewhat limited. A much more comprehensive mapping of the parameter space for the time-independent flow and transport parameters was performed by Petrovay and Talafha (2019). The observational constraints applied in that study were based on phase differences in the temporal variation of various measures of the solar magnetic field. An interesting further possibility to constrain the parameters was pointed out by Petrie (2023; 2024), who suggested that characteristic shapes of the flux patterns originating from decaying active regions at higher latitudes may serve as sensitive tests of the transport parameters. Exploiting these constraints in a 2D flux transport model is one potential direction for a future extension of this work.

5. Conclusion

In this study, we used the 1D surface flux transport model to study the effect of nonlinear surface inflows into activity belts in solar cycle modulation. We used a modified meridional flow perturbation profile presented byNagy et al. (2017) to represent the surface inflows whose amplitudes vary within a cycle depending on the magnetic activity.

Our results confirmed that introducing surface inflows into the solar dynamo will provide a polar field within an average cycle polar field of $\pm 1\sigma$, and including LQ and TQ together with inflows will give a more balanced impact on the polar field. Results show that having inflows will decrease the strength of the global dipole moment in the presence or absence of latitude quenching, and for different allowed parameter combinations. Our model yielded results that closely resemble those of the 2×2D dynamo model. A reduction of $10-25\%$ was observed depending on the chosen model parameters.

Including inflows into the model shows that the relative importance of LQ vs. inflows is inversely correlated with the chosen parameters (u_0, η, and τ) and hence, on the dynamo effectivity range (λ_R), with lower values depending on the initial amplitude of the surface inflow.

When there is no decay term ($\tau = \infty$), the introduction of the inflows into the model results in a less significant net contribution to the dipole moment. In other words, a decay term is essential for the model.

For the used inflow profile, the anticipated modulation of the source was expected to persist within the linear regions, similar to the TQ case. However, relying on fitting to determine the significance of LQ vs. inflows suggests that the assumption of a linear dependence of source modulation on cycle amplitude is somewhat simplistic. This shows a possible nonlinear relationship between the surface inflows and the solar dipole moment, suggesting a potential nonlinear mechanism contributing to the saturation of the global dynamo within the Babcock-Leighton framework.

TQ dominates over LQ for low λ_R, after that a transition for LQ gradually dominates TQ, adding inflows gives an earlier transition of domination from TQ to LQ. However, for no decay term, the transition will occur a little bit later.

A plausible further extension of this work would consider solar cycle scale variation of the order of 2 m s^{-1} as the third near-surface meridional flow component, in addition to the constant baseline flow profile and the variations due to inflows around active regions.

Declarations

References

Babcock, H.W., Babcock, H.D.: 1955, The Sun's Magnetic Field, 1952-1954. *Astrophysical Journal, vol. 121, p. 349* **121**, 349.

Baumann, I., Schmitt, D., Schüssler, M., Solanki, S.: 2004, Evolution of the large-scale magnetic field on the solar surface: a parameter study. *A&A* **426**, 1075.

Bhowmik, P., Nandy, D.: 2018, Prediction of the strength and timing of sunspot cycle 25 reveal decadal-scale space environmental conditions. *Nat. Commun.* **9**, 5209. DOI. ADS.

Bhowmik, P., Jiang, J., Upton, L., Lemerle, A., Nandy, D.: 2023, Physical models for solar cycle predictions. *Space Sci. Rev.* **219**, 40.

Cameron, R., Schüssler, M.: 2010, Changes of the solar meridional velocity profile during cycle 23 explained by flows toward the activity belts. *ApJ* **720**, 1030.

Cameron, R., Schüssler, M.: 2012, Are the strengths of solar cycles determined by converging flows towards the activity belts? *A&A* **548**, A57.

Cameron, R.H., Schüssler, M.: 2016, The turbulent diffusion of toroidal magnetic flux as inferred from properties of the sunspot butterfly diagram. *Astron. Astrophys.* **591**, A46. DOI. ADS.

Cameron, R.H., Schmitt, D., Jiang, J., Işık, E.: 2012, Surface flux evolution constraints for flux transport dynamos. *A&A* **542**, A127.

Dasi-Espuig, M., Solanki, S.K., Krivova, N.A., Cameron, R., Peñuela, T.: 2010, Sunspot group tilt angles and the strength of the solar cycle. *Astron. Astrophys.* **518**, A7. DOI. ADS.

D'silva, S., Choudhuri, A.: 1993, A theoretical model for tilts of bipolar magnetic regions. *A&A* **272**, 621.

Finley, A.J., Brun, A., Strugarek, A., Cameron, R.: 2024, How well does surface magnetism represent deep Sun-like star dynamo action? *Astronomy & Astrophysics* **684**, A92.

Gizon, L.: 2004, Helioseismology of time-varying flows through the solar cycle. *Sol. Phys.* **224**, 217.

Gizon, L., Duvall, T., Larsen, R.: 2001, Probing surface flows and magnetic activity with time-distance helioseismology. In: *Symposium-International Astronomical Union* **203**, 189. Cambridge University Press.

González Hernández, I., Kholikov, S., Hill, F., Howe, R., Komm, R.: 2008, Subsurface meridional circulation in the active belts. *Sol. Phys.* **252**, 235.

Hathaway, D.H., Rightmire, L.: 2010, Variations in the Sun's meridional flow over a solar cycle. *Science* **327**, 1350.

Hathaway, D.H., Upton, L.A.: 2016, Predicting the amplitude and hemispheric asymmetry of solar cycle 25 with surface flux transport. *Journal of Geophysical Research: Space Physics* **121**, 10.

Iijima, H., Hotta, H., Imada, S., Kusano, K., Shiota, D.: 2017, Improvement of solar-cycle prediction: Plateau of solar axial dipole moment. *Astron. Astrophys.* **607**, L2. DOI. ADS.

Jha, B.K., Karak, B.B., Mandal, S., Banerjee, D.: 2020, Magnetic field dependence of bipolar magnetic region tilts on the Sun: Indication of tilt quenching. *ApJL* **889**, L19.

Jiang, J.: 2020, Nonlinear Mechanisms that Regulate the Solar Cycle Amplitude. *Astrophys. J.* **900**, 19. DOI. ADS.

Jiang, J., Cao, J.: 2018, Predicting solar surface large-scale magnetic field of Cycle 24. *JASTP* **176**, 34. DOI. ADS.

Jiang, J., Işik, E., Cameron, R., Schmitt, D., Schüssler, M.: 2010, The effect of activity-related meridional flow modulation on the strength of the solar polar magnetic field. *ApJ* **717**, 597.

Jiang, J., Cameron, R.H., Schmitt, D., Schüssler, M.: 2011, The solar magnetic field since 1700. I. Characteristics of sunspot group emergence and reconstruction of the butterfly diagram. *Astron. Astrophys.* **528**, A82. DOI. ADS.

Jiang, J., Hathaway, D., Cameron, R., Solanki, S., Gizon, L., Upton, L.: 2014, Magnetic flux transport at the solar surface. *Space Sci. Rev.* **186**, 491.

Jiang, J., Wang, J.-X., Jiao, Q.-R., Cao, J.-B.: 2018, Predictability of the solar cycle over one cycle. *ApJ* **863**, 159.

Jiao, Q., Jiang, J., Wang, Z.-F.: 2021, Sunspot tilt angles revisited: Dependence on the solar cycle strength. *A&A* **653**, A27.

Käpylä, P., Korpi, M., Ossendrijver, M., Stix, M.: 2006, Magnetoconvection and dynamo coefficients-III. α-effect and magnetic pumping in the rapid rotation regime. *Astronomy & Astrophysics* **455**, 401.

Karak, B.B.: 2020, Dynamo Saturation through the Latitudinal Variation of Bipolar Magnetic Regions in the Sun. *Astrophys. J. Lett.* **901**, L35. DOI. ADS.

Komm, R., Howard, R., Harvey, J.: 1993, Meridional flow of small photospheric magnetic features. *Sol. Phys.* **147**, 207.

Lemerle, A., Charbonneau, P.: 2017, A Coupled 2 × 2D Babcock-Leighton Solar Dynamo Model. II. Reference Dynamo Solutions. *Astrophys. J.* **834**, 133. DOI. ADS.

Martin-Belda, D., Cameron, R.H.: 2016, Surface flux transport simulations: Effect of inflows toward active regions and random velocities on the evolution of the Sun's large-scale magnetic field. *A&A* **586**, A73.

Martin-Belda, D., Cameron, R.H.: 2017, Inflows towards active regions and the modulation of the solar cycle: A parameter study. *A&A* **597**, A21.

Nagy, M., Lemerle, A., Charbonneau, P.: 2020, Impact of nonlinear surface inflows into activity belts on the solar dynamo. *JSWSC* **10**, 62. DOI. ADS.

Nagy, M., Lemerle, A., Labonville, F., Petrovay, K., Charbonneau, P.: 2017, The effect of "Rogue" active regions on the solar cycle. *Sol. Phys.* **292**, 1.

Ossendrijver, M., Stix, M., Brandenburg, A., Rüdiger, G.: 2002, Magnetoconvection and dynamo coefficients-II. Field-direction dependent pumping of magnetic field. *Astronomy & Astrophysics* **394**, 735.

Petrie, G.J.D.: 2023, Polar Photospheric Magnetic Field Evolution and Global Flux Transport. *Sol. Phys.* **298**, 43. DOI.

Petrie, G.J.: 2024, Global solar photospheric and coronal magnetic field over activity cycles 21–25. *Journal of Space Weather and Space Climate* **14**, 5.

Petrovay, K.: 2020, Solar cycle prediction. *Living Rev. Sol. Phys.* **17**, 2. DOI. ADS.

Petrovay, K., Talafha, M.: 2019, Optimization of surface flux transport models for the solar polar magnetic field. *Astron. Astrophys.* **632**, A87. DOI. ADS.

Petrovay, K., Nagy, M., Yeates, A.R.: 2020, Towards an algebraic method of solar cycle prediction. I. Calculating the ultimate dipole contributions of individual active regions. *JSWSC* **10**, 50. DOI. ADS.

Schrijver, C.J., De Rosa, M.L., Title, A.M.: 2002, What Is Missing from Our Understanding of Long-Term Solar and Heliospheric Activity? *Astrophys. J.* **577**, 1006. DOI. ADS.

Talafha, M., Nagy, M., Lemerle, A., Petrovay, K.: 2022, Role of observable nonlinearities in solar cycle modulation. *A&A* **660**, A92.

Wang, Y.-M., Sheeley, N.: 2009, Understanding the geomagnetic precursor of the solar cycle. *The Astrophysical Journal* **694**, L11.

Whitbread, T., Yeates, A.R., Muñoz-Jaramillo, A., Petrie, G.J.D.: 2017, Parameter optimization for surface flux transport models. *Astron. Astrophys.* **607**, A76. DOI. ADS.

Yeates, A.R., Cheung, M.C., Jiang, J., Petrovay, K., Wang, Y.-M.: 2023, Surface Flux Transport on the Sun. *Space Sci. Rev.* **219**, 31.